

Primary-Filling $e/3$ Quasiparticle Interferometer

F. E. Camino, Wei Zhou, and V. J. Goldman

Department of Physics, Stony Brook University, Stony Brook, NY 11794-3800, USA

(Received 6 September 2006)

We report experimental realization of a quasiparticle interferometer where the entire system is in $1/3$ primary fractional quantum Hall state. The interferometer consists of chiral edge channels coupled by quantum-coherent tunneling in two constrictions, thus enclosing an Aharonov-Bohm area. We observe magnetic flux and charge periods h/e and $e/3$, equivalent to creation of one quasielectron in the island. Quantum theory predicts a $3h/e$ flux period for charge $e/3$, integer statistics particles. Accordingly, the observed periods demonstrate the anyonic statistics of Laughlin quasiparticles.

A clean system of 2D electrons subjected to high magnetic field at low temperatures condenses into the fractional quantum Hall (FQH) fluids [1-4]. An exact filling f FQH condensate is incompressible and gapped, the celebrated examples of FQH condensates are the Laughlin many-electron wave functions for the *primary* fillings $f=1/(2j+1)$, with j an integer. The elementary charged excitations of an FQH condensate are the Laughlin quasiparticles. Deviation of the filling factor from the exact value is achieved by excitation of either quasielectrons or quasiholes out of the condensate; at such fillings the ground state of an FQH fluid consists of the quasiparticle-containing condensate. The FQH quasiparticles have fractional electric charge [2-6] and obey fractional statistics [7-10].

Fractionally charged quasiparticles were first observed in quantum antidot experiments, where quasiperiodic resonant conductance peaks are observed when the occupation of the antidot is incremented by one quasiparticle [6,11,12]. A quantum antidot is a small potential hill, defined lithographically in the 2D electron system. Complementary geometry where a 2D electron island is defined by two nearly open constrictions comprises an electron interferometer [13-16]. Recently, we reported realization of a quasiparticle interferometer where $e/3$ quasiparticles of the $f=1/3$ FQH fluid execute a closed path around an island of the $f=2/5$ fluid [9,10,17]. The interference fringes are observed as conductance oscillations as a function of the magnetic flux through the island, that is, the Aharonov-Bohm effect. The observed flux and charge periods, $\Delta_\Phi = 5h/e$ and $\Delta_Q = 2e$, are equivalent to excitation of ten $q=e/5$ quasiparticles of the $2/5$ fluid. Such superperiodic $\Delta_\Phi > h/e$ had never been reported before in any system. The superperiod is interpreted as imposed by the topological order of the underlying FQH condensates [18], manifested by the anyonic statistical interaction of the quasiparticles [19,20].

Our present experiment utilizes a comparable quasiparticle interferometer, but with much less depleted constrictions, Fig. 1. This results in the entire island being at the primary filling $f=1/3$ under coherent tunneling conditions, so that $e/3$ quasiparticles execute a closed path around an island of the $1/3$ FQH fluid containing other $e/3$ quasiparticles. This simpler regime should help theoretical consideration of the quasiparticle interferometer physics. For the first time in such devices we report interferometric oscillations. The flux and charge periods of $\Delta_\Phi = h/e$ and $\Delta_Q = e/3$, respectively, correspond to addition of one quasiparticle to the area enclosed by the interference path. These periods are the same as in quantum antidots, but the quasiparticle path encloses no electron vacuum in the interferometer. The results are consistent

with the Berry phase quantization condition that includes both Aharonov-Bohm and anyonic statistical contributions.

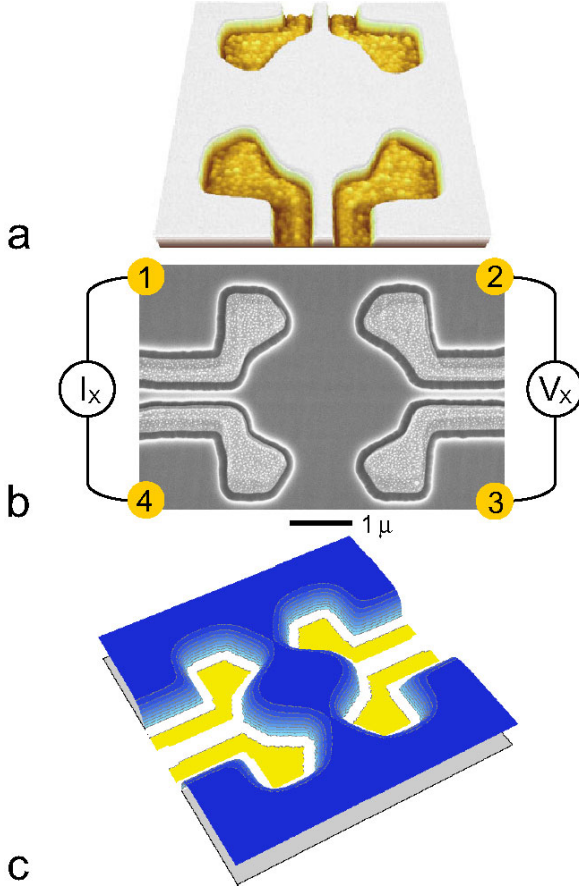


FIG. 1. The $e/3$ quasiparticle interferometer device. (a),(b) Atomic force and scanning electron micrographs. (c) Illustration of the 2D electron density profile. Four front-gates are deposited in shallow etch trenches. Depletion potential of the trenches defines the electron island. The chiral edge channels follow equipotentials at the periphery of the undepleted 2D electrons. Tunneling occurs at the saddle points in the two constrictions. The edge channel path is closed by the tunneling links, thus forming the interferometer. The backgate (not shown) extends over the entire sample.

The interferometer devices were fabricated from low disorder AlGaAs/GaAs heterojunctions. After a shallow 130 nm wet etching, Au/Ti front-gate metal was deposited in the etch trenches, followed by lift-off, Fig. 1(a,b). Samples were mounted on sapphire substrates with In metal, which serves as the backgate, and were cooled in a dilution refrigerator to 10.2 mK bath temperature, calibrated by nuclear orientation thermometry. Extensive cold filtering cuts the electromagnetic environment incident on the sample, allowing to achieve electron temperature ≤ 15 mK in an interferometer device [21]. Four-terminal resistance $R_{XX} = V_X / I_X$ was measured with 50 pA ($f = 1/3$) or 200 pA ($f = 1$), 5.4 Hz ac current injected at contacts 1 and 4. The resulting voltage, including the interference signal, was detected at contacts 2 and 3.

The etch trenches define two $1.25\ \mu\text{m}$ wide constrictions, which separate an approximately circular electron island from the 2D bulk. Moderate front-gate voltages V_{FG} are used to fine tune the constrictions for symmetry of the tunnel coupling and to increase the oscillatory interference signal. The shape of the electron density profile is predominantly determined by the etch trench depletion, illustrated in Fig. 1(c). For the 2D bulk density $n_B = 1.25 \times 10^{11}\ \text{cm}^{-2}$ there are $\sim 3,500$ electrons in the island. The depletion potential has saddle points in the constrictions, and so has the resulting density profile.

In a quantizing field B the counterpropagating edge channels pass near the saddle points, where tunneling may occur. Thus, in the range of B where the interference oscillations are

observed, the filling of the edge channels is determined by the saddle point filling [17]. This allows to determine the saddle point density from the $R_{XX}(B)$ and $R_{XY}(B)$ magnetotransport, Fig. 2(a). The Landau level filling $\nu = hn/eB$ is proportional to the electron density n , accordingly the constriction ν is lower than the bulk ν_B in a given B . The island center n is estimated to be 3% less than n_B at $V_{FG} = 0$, the constriction - island center density difference is $\sim 7\%$. Thus, the whole island is on the same plateau for strong quantum Hall states with wide plateaus, such as $f=1$ and $1/3$. While ν is a variable, the quantum Hall exact filling f is a quantum number defined by the quantized Hall resistance as $f = h/e^2 R_{XY}$.

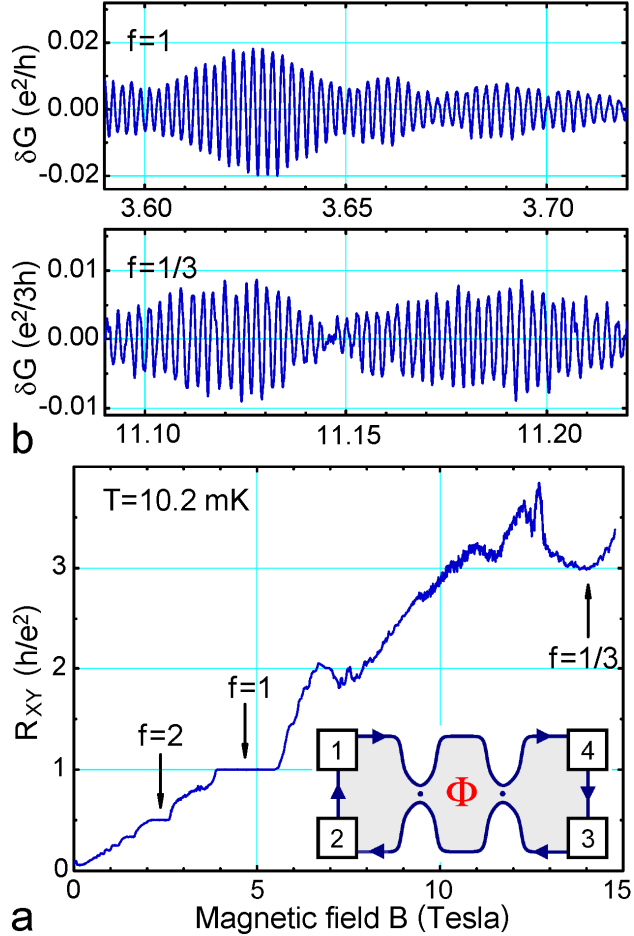


FIG. 2. (a) The Hall resistance of the interferometer device at zero front-gate voltage. The quantized plateaus allow to determine the filling factor in the constrictions. Inset: the chiral edge channel electron interferometer concept; dots stand for tunneling. (b) Representative interference conductance oscillations for electrons ($f=1$) and for $e/3$ quasiparticles ($f=1/3$). The magnetic flux period is $\Delta\Phi = h/e$ in both regimes. Negative front-gate voltage, applied to increase the oscillation amplitude, shifts the oscillations to lower B .

In the integer quantum Hall regime the Aharonov-Bohm ring is formed by the two counter-propagating chiral edge channels passing through the constrictions. The backscattering occurs by quantum tunneling at the saddle points in the constrictions, Fig. 1, which complete the interference path. The relevant particles are electrons of charge $-e$ and Fermi statistics, thus we can obtain an absolute calibration of the Aharonov-Bohm path area and the backgate action of the interferometer. Figure 2(b) shows conductance oscillations for $f=1$; analogous oscillations were also observed for $f=2$. The oscillatory conductance $\delta G = \delta R_{XX} / R_{XY}^2$ is calculated from the R_{XX} data after subtracting a smooth background. The smooth background has two contributions: the bulk conduction at ν_B outside the bulk plateau regions, and the non-oscillatory

inter-edge backscattering conductance in the interferometer. Extrapolated to $V_{FG} = 0$ [14,17], the $f=1$ magnetic field oscillation period is $\Delta_B = 1.86$ mT. This gives the interferometer path area $S = h/e\Delta_B = 2.22 \mu\text{m}^2$, the radius $r = 840$ nm.

In the FQH regime, $f=1/3$, we observe the interferometric oscillations as a function of magnetic field, Fig. 2(b). This is the first experimental observation of $e/3$ quasiparticle interference oscillations when the island filling is $1/3$ throughout. Extrapolated to $V_{FG} = 0$, the magnetic field oscillation period is $\Delta_B = 1.93$ mT. Assuming the flux period is $\Delta_\Phi = h/e$, this gives the interferometer path area $S = h/e\Delta_B = 2.14 \mu\text{m}^2$, the radius $r = 825$ nm. The island edge ring area is strictly determined by the requirement that the edge channels pass near the saddle points in the constrictions. Classically, increasing B by a factor of ~ 3 does not affect the electron density distribution in the island at all. Quantum corrections are expected to be small for a large island containing $\sim 3,500$ electrons. Indeed, the $f=1/3$ interferometer path area is within $\pm 3\%$ of the integer value, where $\pm 3\%$ is the estimated experimental uncertainty. The integer regime oscillations have an h/e fundamental flux period, we conclude that the flux period of the $1/3$ FQH oscillations is also $\Delta_\Phi = h/e$.

We use the backgate technique [6,11] to directly measure the charge period in the fractional regime. We calibrate the backgate action $\delta Q / \delta V_{BG}$, where Q is the electronic charge within the Aharonov-Bohm path. The calibration is done by evaluation of the coefficient α using the experimental oscillation periods in

$$\Delta_Q = \alpha(\Delta_{V_{BG}} / \Delta_B), \quad (1)$$

setting $\Delta_Q = e$ in the integer regime. Note that Eq. (1) normalizes the backgate voltage periods by the experimental B -periods, approximately canceling the variation in device area, for example, due to a front-gate bias. The coefficient α in Eq. (1) is known *a priori* in quantum antidots to a good accuracy because the antidot is completely surrounded by the quantum Hall fluid [6, 11]. But, in an interferometer, the island is separated from the 2D electron plane by the front-gate etch trenches, so that its electron density is not expected to increase by precisely the same amount as n_B , which necessitates the calibration.

Figure 3 shows the oscillations as a function of V_{BG} for $f=1$ and $1/3$ and the analogous oscillations as a function of B . At each filling, the front-gate voltage is the same for the (vs V_{BG} , vs B) set. The $f=1$ period $\Delta_{V_{BG}}$ corresponds to increment $\Delta_N = 1$ in the number of electrons within the interference path. We obtain $\Delta_{V_{BG}} = 315$ mV, $\Delta_B = 2.34$ mT, and the ratio $\Delta_{V_{BG}} / \Delta_B = 134.3$ V/T (front-gate $V_{FG} = -210$ mV for these data). This period ratio is 0.92 of that obtained in quantum antidots [11], consistent with expectation. For the $1/3$ FQH oscillations we obtain $\Delta_{V_{BG}} = 117.3$ mV, $\Delta_B = 2.66$ mT, and the ratio $\Delta_{V_{BG}} / \Delta_B = 44.1$ V/T (front-gate $V_{FG} = -315$ mV for these data). Using the integer calibration in the same device, the $e/3$ quasiparticle experimental charge period is $\Delta_Q = 0.328e$, some 1.7% less than $e/3$. To the first order, using the $\Delta_{V_{BG}} / \Delta_B$ ratio technique cancels dependence of the V_{BG} and B periods on the

interferometer area (and V_{FG} bias). The scatter of the quasiparticle charge values obtained from several matched data sets in this experimental run is $\pm 3\%$.

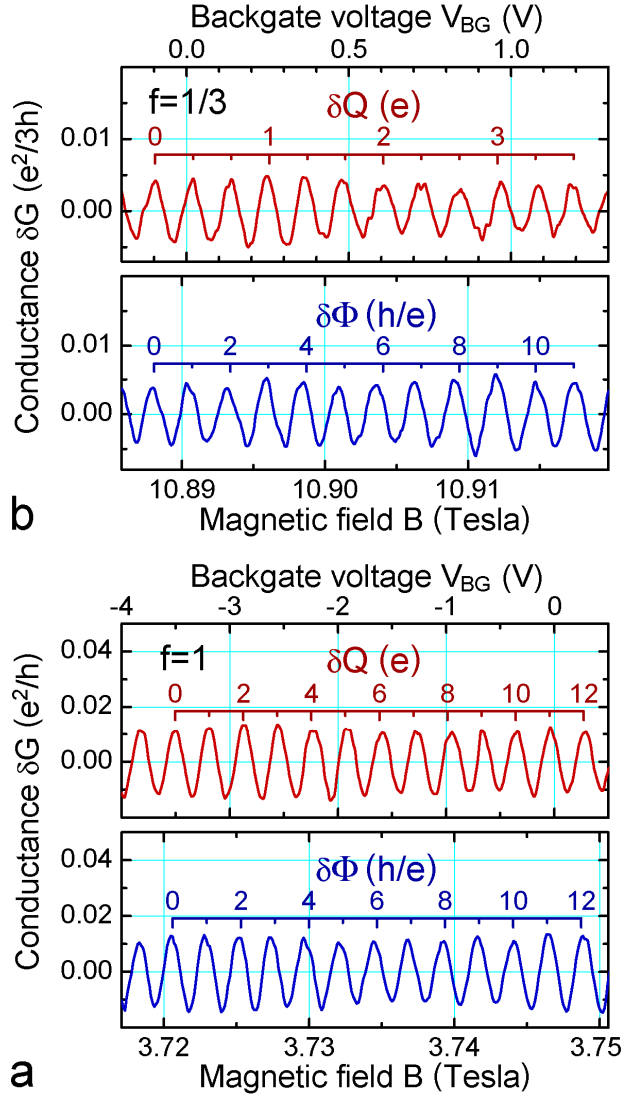


FIG. 3. Matched sets of oscillatory conductance data giving the $e/3$ charge period. (a) The interferometer device is calibrated using the conductance oscillations for electrons, $f = 1$. (b) This calibration gives the charge period for the Laughlin quasielectrons $q = (0.328 \pm 0.010)e$. The magnetic flux period $\Delta_\Phi = h/e$, the same in both regimes, implies anyonic statistics of the fractionally charged quasiparticles.

These experimental results can be understood as follows. The essential physics of the quasiparticle interferometer is discussed in Refs. [22-24,16,10]. The experimental periods are the same as in quantum antidots, comprising addition of one quasiparticle only. When filling $\nu < 1/3$, as in quantum antidots, addition of flux h/e to an area occupied by the $1/3$ FQH condensate creates a quantized vortex, an $e/3$ quasihole. However, the interferometric oscillations are observed to occur at filling $\nu > 1/3$, when quasielectrons are added to the condensate. This is consistent with the principal difference between the $e/3$ interferometer and the antidots being that in quantum antidots the FQH fluid surrounds electron vacuum, while in the present interferometer the island contains the $1/3$ FQH fluid everywhere within the interference path. Addition of flux reduces the number of $-e/3$ quasielectrons, the electron system is not the same as prior to flux addition, the added flux cannot be annulled by a singular gauge transformation [25]. Another subtle difference is that a single quasihole can always be created in the $1/3$ condensate, while creation of a single quasielectron is not possible in an

isolated FQH droplet, for example [26]. Periods of $\Delta_\Phi = 3h/e$ and $\Delta_Q = e$ have been predicted in certain 1/3 FQH non-equilibrium models [22,23,27,16]. We therefore discuss our experimental results via quasielectron configurations in the FQH ground state, as a more restrictive case.

In an unbounded FQH fluid, changing ν away from the exact filling f is accomplished by creation of quasiparticles; the ground state consists of the $\nu = f$ condensate and the matching density of quasiparticles [3-5,24]. Starting at $\nu = f$, changing magnetic field adiabatically maintains the system in thermal equilibrium. The equilibrium electron density, determined by the positively charged donors, is not affected. In present geometry, changing B also changes the flux $\Phi = BS$ through the area S enclosed by the interference path. In the $\nu > 1/3$ regime, decreasing Φ by h/e increases the number of quasielectrons in S by one, $\Delta_N = 1$, and decreases by $+e/3$ the negative FQH condensate charge within S . The quasielectron is created out of the 1/3 condensate, the condensate density changes by $+e/3S$, the charge within the interference path does not alter and still neutralizes the positive donor charge.

This process can be expressed in terms of the Berry phase γ of the encircling $-e/3$ quasielectron, which includes the Aharonov-Bohm and the statistical contributions [23,12]. When there is only one quasiparticle of charge $q = \pm e/3$ present, its orbitals are quantized by the Aharonov-Bohm condition $\gamma_m = (|q|/\hbar)\Phi_m = 2\pi m$ to enclose flux $\Phi_m = m\hbar/|q|$ with $m = 0, 1, 2, \dots$ [7]. These quantized quasiparticle orbitals enclose $-em$ of the underlying 1/3 condensate charge. When other quasiparticles are present quantization of the Berry phase includes a term describing mutual braiding statistics of the quasiparticles [8], in addition to the Aharonov-Bohm phase. The total phase is quantized in increments of 2π :

$$\Delta_\gamma = \frac{q}{\hbar}\Delta_\Phi + 2\pi\Theta_{1/3}\Delta_N = 2\pi, \quad (2)$$

where $q = -e/3$ is the charge of the interfering quasielectron, and $\Theta_{1/3}$ is the statistics of the $-e/3$ quasielectrons. The first term in Eq. (2) contributes $(-e/3\hbar)(-h/e) = 2\pi/3$, the second term must contribute $4\pi/3$, giving an anyonic statistics $\Theta_{1/3} = 2/3$.

The same Berry phase equation describes the physically different process of the island charging by the backgate. Here, in a fixed B , increasing positive V_{BG} increases the 2D electron density. The period consists of creating one $-e/3$ quasielectron out of the 1/3 condensate within the interference path, which causes the path to shrink by the area containing flux h/e . This is possible because the condensate is not isolated from the 2D bulk electron system, there is no Coulomb blockade, and the condensate charge within the interference path can increment by $+e/3$, any fractional charge imbalance ultimately supplied from the contacts. Thus, an $-e/3$ quasielectron is excited out of the condensate, $\Delta_N = 1$, the fixed condensate density is restored from the contacts, the interference path shrinks by area h/eB so that flux $\Delta_\Phi = -h/e$ in Eq. (2), FQH fluid charge within the interference path does not neutralize the donors by $-e/3$.

In conclusion, we realized a novel primary-filling $e/3$ quasiparticle interferometer where an $e/3$ quasiparticle executes a closed path around an island containing the 1/3 FQH fluid only. The central results obtained, the flux and charge periods of $\Delta_\Phi = h/e$ and $\Delta_Q = e/3$ are robust. Both the Aharonov-Bohm and the charging periods accurately correspond to excitation of one

– $e/3$ quasielectron within the interference path and are interpreted as imposed by the anyonic braiding statistics of FQH quasiparticles.

We acknowledge discussions with D. V. Averin and B. I. Halperin. This work was supported in part by the NSF and by U.S. ARO.

1. D. C. Tsui, H. L. Stormer, and A. C. Gossard, Phys. Rev. Lett. **48**, 1559 (1982).
2. R. B. Laughlin, Phys. Rev. Lett. **50**, 1395 (1983).
3. R. B. Laughlin, Rev. Mod. Phys. **71**, 863 (1999).
4. *The Quantum Hall Effect*, 2nd Ed., edited by R. E. Prange and S. M. Girvin (Springer, NY, 1990); D. Yoshioka, *The Quantum Hall Effect* (Springer, 2002).
5. F. D. M. Haldane, Phys. Rev. Lett. **51**, 605 (1983).
6. V. J. Goldman and B. Su, Science **267**, 1010 (1995).
7. B. I. Halperin, Phys. Rev. Lett. **52**, 1583 (1984).
8. D. Arovas, J. R. Schrieffer, and F. Wilczek, Phys. Rev. Lett. **53**, 722 (1984).
9. F. E. Camino, W. Zhou, and V. J. Goldman, Phys. Rev. Lett. **95**, 246802 (2005).
10. F. E. Camino, W. Zhou, and V. J. Goldman, Phys. Rev. B **72**, 075342 (2005).
11. V. J. Goldman, I. Karakurt, J. Liu, and A. Zaslavsky, Phys. Rev. B **64**, 085319 (2001).
12. V. J. Goldman, J. Liu, and A. Zaslavsky, Phys. Rev. B **71**, 153303 (2005).
13. B. J. van Wees *et al.*, Phys. Rev. Lett. **62**, 2523 (1989); L. P. Kouwenhoven *et al.*, Surf. Science **229**, 290 (1990).
14. F. E. Camino, W. Zhou, and V. J. Goldman, Phys. Rev. B **72**, 155313 (2005).
15. C. M. Markus, private communication.
16. C. de C. Chamon *et al.*, Phys. Rev. B **55**, 2331 (1997).
17. W. Zhou, F. E. Camino, and V. J. Goldman, Phys. Rev. B **73**, 245322 (2006).
18. X. G. Wen, Adv. Phys. **44**, 405 (1995); T. Senthil and M. P. A. Fisher, Phys. Rev. B **62**, 7850 (2000).
19. J. M. Leinaas and J. Myrheim, Nuovo Cimento **37B**, 1 (1977).
20. F. Wilczek, Phys. Rev. Lett. **48**, 1144 (1982); Phys. Rev. Lett. **49**, 957 (1982).
21. F. E. Camino, W. Zhou, and V. J. Goldman, Phys. Rev. B **74**, 115301 (2006).
22. S. A. Kivelson and V. L. Pokrovsky, Phys. Rev. B **40**, 1373 (1989).
23. S. A. Kivelson, Phys. Rev. Lett. **65**, 3369 (1990).
24. V. J. Goldman, cond-mat/0605614.
25. C. N. Yang, Rev. Mod. Phys. **34**, 694 (1962); R. B. Laughlin, Phys. Rev. B **23**, 5632 (1981).
26. A. Cappelli, C. Mendez, J. Simonin, and G. R. Zemba, Phys. Rev. B **58**, 16291 (1998); E. V. Tsiper, Phys. Rev. Lett. **97**, 076802 (2006).
27. Y. Gefen and D. J. Thouless, Phys. Rev. B **47**, 10423 (1993).